Clinical Cancer Research

Single-Cell Dynamics Determines Response to CDK4/6 Inhibition in Triple-Negative Breast Cancer

Uzma S. Asghar[1], Alexis R. Barr[2], Ros Cutts[1], Matthew Beaney[1], Irina Babina[1], Deepak Sampath[3], Jennifer Giltnane[3], Jennifer Arca Lacap[3], Lisa Crocker[3], Amy Young[3], Alex Pearson[1], Maria Teresa Herrera-Abreu[1], Chris Bakal[2], and Nicholas C. Turner[1,4]

Abstract

Purpose: Triple-negative breast cancer (TNBC) is a heterogeneous subgroup of breast cancer that is associated with a poor prognosis. We evaluated the activity of CDK4/6 inhibitors across the TNBC subtypes and investigated mechanisms of sensitivity.

Experimental Design: A panel of cell lines representative of TNBC was tested for *in vitro* and *in vivo* sensitivity to CDK4/6 inhibition. A fluorescent CDK2 activity reporter was used for single-cell analysis in conjunction with time-lapse imaging.

Results: The luminal androgen receptor (LAR) subtype of TNBC was highly sensitive to CDK4/6 inhibition both *in vitro* ($P < 0.001$ LAR vs. basal-like) and *in vivo* in MDA-MB-453 LAR cell line xenografts. Single-cell analysis of CDK2 activity demonstrated differences in cell-cycle dynamics between LAR and basal-like cells. Palbociclib-sensitive LAR cells exit mitosis with low levels of CDK2 activity, into a quiescent state that requires CDK4/6 activity for cell-cycle reentry. Palbociclib-resistant basal-like cells exit mitosis directly into a proliferative state, with high levels of CDK2 activity, bypassing the restriction point and the requirement for CDK4/6 activity. High CDK2 activity after mitosis is driven by temporal deregulation of cyclin E1 expression. CDK4/6 inhibitors were synergistic with PI3 kinase inhibitors in *PIK3CA*-mutant TNBC cell lines, extending CDK4/6 inhibitor sensitivity to additional TNBC subtypes.

Conclusions: Cell-cycle dynamics determine the response to CDK4/6 inhibition in TNBC. CDK4/6 inhibitors, alone and in combination, are a novel therapeutic strategy for specific subgroups of TNBC. *Clin Cancer Res; 23(18); 5561–72. ©2017 AACR.*

Introduction

The CDK4/6–RB1 axis controls transition through the restriction point in the G_1 phase of the cell cycle, and cancers frequently subvert the regulation of this axis to promote proliferation (1, 2). CDK4/6 inhibition is a proven therapeutic strategy for estrogen receptor–positive (ER^+) breast cancers (3, 4), with selective CDK4/6 inhibitors (palbociclib and ribociclib) demonstrating substantial improvements in progression-free survival [PALOMA1 (3), PALOMA2 (5), PALOMA3 (4) and MONALEESA-2 (6)] in phase two and three clinical trials.

Triple-negative breast cancer (TNBC) is an aggressive subtype of breast cancer, which is associated with a poor prognosis. Although TNBC may be sensitive to chemotherapy, there is still a substantial need to identify novel targeted therapeutic strategies. TNBC is a heterogeneous group of tumors and gene expression profiling has identified distinct subgroups (7, 8), including luminal androgen receptor (LAR), mesenchymal stem like (MSL), mesenchymal (MES), and basal-like (7). The majority of TNBC fall within the dominant basal-like and MES subgroups. TNBC are a highly proliferative group of tumors enriched for high expression of cell-cycle genes (7), yet as a heterogeneous subtype, are considered to be resistant to CDK4/6 inhibition (9), as are many other tumor types.

The determinants of sensitivity to CDK4/6 inhibition are poorly understood. Loss of retinoblastoma protein (RB1) causes resistance to CDK4/6 inhibition (10); however, for the majority of cancers, the factors that determine sensitivity or resistance to CDK4/6 inhibitors are unclear. Recent studies of cell-cycle dynamics have redefined our understanding of the G_1–S phase transition in asynchronously dividing cells (11–13), with cells at mitotic exit entering either a quiescent or an active–proliferative state (12, 13). Here we show that cell-cycle exit into a quiescent or proliferative state is a major factor determining sensitivity to CDK4/6 inhibitors. We identify subgroups of TNBC that are highly sensitive to CDK4/6 inhibition, and using a CDK2 activity live-cell reporter (12), we show that CDK2 activity after mitotic exit dictates sensitivity to CDK4/6 inhibition.

Materials and Methods

Cell lines

Cell lines were obtained from ATCC or Asterand and maintained according to the manufacturer's instructions. Cell lines

[1]Breast Cancer Now Toby Robins Research Centre, Institute of Cancer Research, London, United Kingdom. [2]The Division of Cancer Biology, Institute of Cancer Research, London, United Kingdom. [3]Department of Translational Oncology, Genentech (Roche Group), Genentech, South San Francisco, California. [4]Breast Unit, The Royal Marsden Hospital, London, United Kingdom.

Note: Supplementary data for this article are available at Clinical Cancer Research Online (http://clincancerres.aacrjournals.org/).

Corresponding Author: Nicholas C. Turner, Institute of Cancer Research and Royal Marsden Hospital, 237 Fulham Road, London SW3 6JB, United Kingdom. Phone: 4420-7352-8133; Fax: 4420-7153-5340; E-mail: nicholas.turner@icr.ac.uk

doi: 10.1158/1078-0432.CCR-17-0369

Translational Relevance

Currently, there are no effective targeted therapies for triple-negative breast cancer (TNBC). We show that the luminal androgen receptor subtype of TNBC is highly sensitive to CDK4/6 inhibition whereas basal-like TNBC tumors are resistant. Differential sensitivity of TNBC subtypes to CDK4/6 inhibition is shown to be a result of cells exiting mitosis into an active proliferating or a quiescent state. Basal-like TNBCs have a high proportion of active proliferating cells that are resistant to CDK4/6 inhibition, which is promoted by dysregulation of cyclin E1 expression. Our results identify novel therapeutic approaches for TNBC and identify mechanisms of sensitivity to CDK4/6 inhibitors.

were banked in multiple aliquots on receipt, identity confirmed by short tandem repeat (STR) profiling with the PowerPlex 1.2 System (Promega) and tested for mycoplasma every two weeks. After extracting cells from liquid nitrogen, the cell lines were passaged twice prior to use in experiments.

Palbociclib-resistant MFM223pR cells were generated by chronic exposure to increasing concentrations of palbociclib (100, 250, 500, 1,000 nmol) over 4 months. Drug treatments were replaced every 3–4 days with fresh media.

Antibodies, reagents, and constructs

Phospho-RB1 S807/811 (8516), RB1 (9313), Cyclin E1 (HE12; 4129), Cyclin E2 (4132), CDK2 (2546), phospho-CDK2 T160 (2561); CDK4 (12790), androgen receptor (3202) were from Cell Signaling Technology; p16 F-12 (SC-1661, Santa Cruz Biotechnology), β-actin (A5441, Sigma); Cyclin E1 (ab33911) and c-myc (ab32072) were from Abcam. Western blot analysis was performed using precast 4%–12% SDS gels, as described previously (14). Densitometry analysis was performed on Western blot films using ImageJ software (NIH, Bethesda, MD), and expressed relative to their corresponding loading control.

Palbociclib (PD-0332991; SelleckChem) was used at 500 nmol, pictilisib (GDC-0941; SelleckChem) at 200 nmol, and taselisib (GDC-0032; Genentech) at 100 nmol, unless otherwise stated. Palbociclib (500 nmol) was used for the majority of experiments as previously (10). No increase in effect on clonogenic growth was observed with doses above 500 nmol (Fig. 1A).

siRNAs were from Thermo Fisher Scientific: *siCCNE1* (#4390824, #4390824, #1299001), *siCON1* (#4390843), *siCON2* (#4390846), and *siUBB* (# 4390824).

The CDK2 activity live-cell sensor (CDK2L-GFP) was generated by cloning the C-terminal PSLD region of Human DNA Helicase B (DHB; 957–1,087 amino acids) into pIRES-GFP puromycin as described previously (11). PCNA was tagged at the N terminus with the modified LSS2-mKate fluorophore to generate LSS2-mKate-PCNA (15).

Cell transfections

For CDK2 activity sensor experiments, cells were transfected with CDK2L-GFP using Lipofectamine 2000 according to the manufacturer's instructions, 48–72 hours prior imaging. For siRNA knockdown experiments, SUM149 cells were transfected with CDK2L-GFP on day 1, then GFP-positive cells (3,000 cells/well) were FACS-sorted into 384-well plate on day 3, and next siRNA transfection using *siCON1* and *siCCNE1* was performed with Lipofectamine RNAiMAX on day 6, followed by time-lapse imaging on days 9–11. As previously demonstrated, the CDK2L-GFP sensor is not phosphorylated by CDK4/6 (11), nor by CDK1 (12).

Time-lapse microscopy

CDK2L-GFP–positive cells were FACS sorted into 384-well plates, with 1,000–3,000 cells seeded per well, 24 hours prior time-lapse imaging. Unless specified, drugs or vehicle were added immediately prior time-lapse experiments. Images were taken on a High-content Opera Spinning Disk confocal microscope (PerkinElmer) with 40× water objective, every 10 minutes, in a NA 0.9 humidified environmental chamber at 37°C and 5% CO_2.

To assess the impact of palbociclib on S-phase entry in SUM149 cells transfected with CDK2L-GFP (Fig. 3A), palbociclib or vehicle (DMSO) was added 8 hours after initiation of time-lapse imaging, with continued imaging for a further 48 hours. Analysis was restricted to cells that underwent mitosis 1–3 hours prior to adding palbociclib or vehicle (DMSO).

To study stability of CDK2 activity in individual cell clones (Fig. 5D; Supplementary Fig. S3A), a single cell was FACS-sorted into each well of a 96-well plate, with single-cell sorting confirmed by bright field microscopy. Plates were incubated for 4 weeks to generate clonal populations. Individual wells were transfected with CDK2L-GFP, and 48 hours later imaged using time-lapse microscopy. All examined clonal populations were STR typed.

Image analysis

Time frames of cells transfected with CDK2L-GFP or LSS2-mKate-PCNA were captured at 10 minutes intervals over a 48–72 hours period. Dynamic changes of CDK2L-GFP or LSS2-mKate-PCNA were manually tracked in individual cells using Volocity (PerkinElmer). To quantify CDK2 activity, both nuclear and perinuclear cytoplasmic CDK2L-GFP intensity were measured simultaneously. CDK2 activity for each time point was calculated as a ratio of mean GFP fluorescent intensity in the cytoplasm divided by the mean GFP fluorescent intensity in the nucleus. For representation, asynchronous single-cell CDK2 activity traces were aligned *in silico* to time of cytokinesis as T0 (time-point = 0). The CDK2 activity traces were smoothed with a window of 4 data points minimizing background noise.

Cell-cycle length (hours) was calculated as the time from first cytokinesis to the second cytokinesis. Unless stated otherwise, postmitotic CDK2 activity was assessed as the CDK2 activity at 2 hours after cytokinesis, as the first time-point across imaged cell lines that allowed reliable quantification of CDK2 activity after reformation of the nuclear membrane and cell flattening (11). Cells with CDK2 activity <0.6 at 2 hours after cytokinesis were defined as $CDK2^{low}$, and cells with CDK2 activity >0.6 at 2 hours points after cytokinesis were defined as $CDK2^{high}$, as described previously (12). In PCNA-tracking experiments, S-phase entry was defined a sharp increase in PCNA intensity with the appearance of nucleoli, as described previously (11). Accumulation of CDK2 activity to a ratio of 1 was used as surrogate for cell-cycle entry, as demonstrated previously (12).

Immunofluorescence

Immediately after time lapse, cells were fixed in 4% paraformaldehyde, washed three times in PBS, permeabilized with 0.2% Triton X-100, and stained at room temperature using mouse and

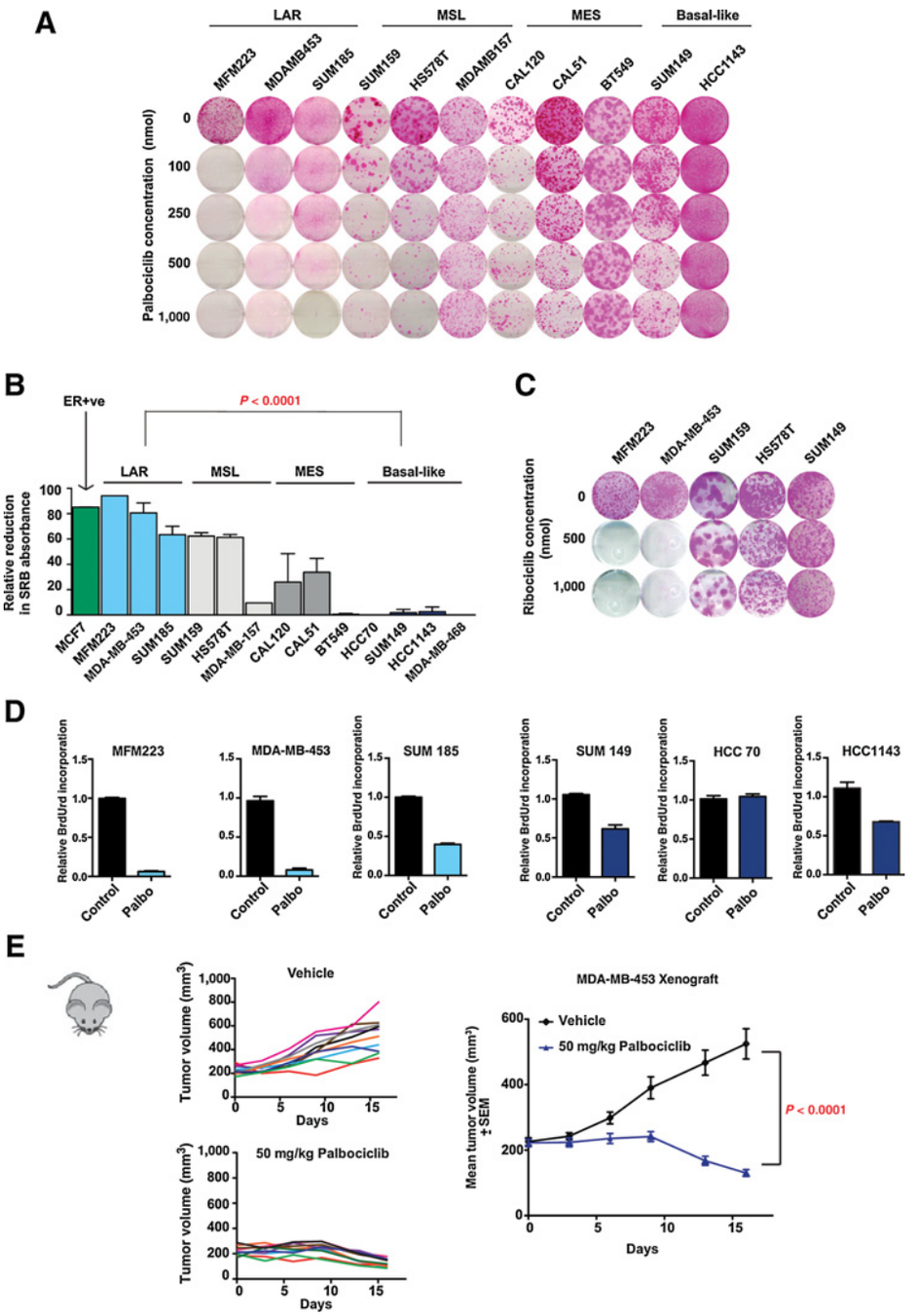

Figure 1.

LAR subgroup of TNBC is sensitive to CDK4/6 inhibition. **A,** Clonogenic assays of TNBC cell lines grown continuously in increasing concentrations of palbociclib, divided by gene expression subtypes: LAR, luminal androgen receptor; MSL, mesenchymal stem-like; MES, mesenchymal and basal-like. All cell lines are *RB1* wild-type except *RB1* mutant BT549. **B,** Sensitivity to 500 nmol palbociclib across 13 TNBC cell lines in clonogenic assays from **A**. LAR subtype is highly sensitive to CDK4/6 inhibition ($P < 0.0001$, Student t test LAR vs. basal-like). ER^+ MCF7 cells are shown as positive control of sensitivity to palbociclib. **C,** Clonogenic assays of 5 TNBC cell lines treated with the CDK4/6 inhibitor ribociclib. **D,** Relative BrdUrd incorporation after 72 hours with or without 500 nmol palbociclib for LAR cell lines (MFM223, MDA-MB-453, and SUM185) and basal-like cell lines (SUM149, HCC70, and HCC1143). **E,** Xenografts of LAR MDA-MB-453 cells, treated daily with vehicle ($n = 10$) or palbociclib ($n = 10$) for 2 weeks. $P < 0.0001$ Student's t test vehicle versus palbociclib at end of treatment.

rabbit primary antibodies, detected with corresponding fluorescent secondary antibodies: anti-mouse Alexa Fluor-555 and anti-rabbit Alexa Fluor-647. Nuclear pixels were measured as an output of intensity for each cell, using Columbus image data storage and analysis system.

Nuclear cyclin E1 protein levels in individual LAR MDA-MB-453 cells and basal-like SUM149 cells 1–2 hours after mitosis (Fig. 4D), was determined by time-lapse imaging of CDK2L-GFP–positive cells (24 hours), followed by immunofluorescence for cyclin E1. Nuclear cyclin E1 protein levels were quantified by measuring the intensity of the immunofluorescence signal with Columbus imaging software, specifically in cells that had undergone mitoses 1–2 hours prior to fixation.

IHC

For IHC analysis of MDA-MB-453 xenografts, tumors were extracted 4 hours after the dose and formalin fixed for IHC. Each sampling time point includes 4 animals per treatment group. IHC was performed on 4-μm thick formalin-fixed, paraffin-embedded tissue sections mounted on glass slides. For cleaved caspase-3 (Cell Signaling Technology), staining was performed on a DAKO autostainer. Sections were treated with DAKO Target Retrieval

(Dako), incubated with primary antibody at 0.12 μg/mL overnight at 4°C followed by biotinylated goat anti-rabbit IgG (Vectorlabs) and detected with Vectastain ABC-HRP (Vectorlabs). For phospho-S6, IHC was performed on the Ventana Discovery XT Autostainer platform (Ventana Medical Systems Inc). The slides were pretreated with CC1, standard time, followed by anti-phospho-S6 (Cell Signaling Technology), incubated at 0.26 μg/mL for 32 minutes at 37°C. The antibody was detected with anti-rabbit-UltraMap (Ventana Medical Systems Inc). Staining was visualized with DAB. Sections were counter stained with hematoxylin, dehydrated, cleared, and coverslipped for viewing.

Assessment of viability and proliferation

All clonogenic assays were conducted in triplicates of 6-well plates, with 1,000–5,000 cells seeded per well 24 hours prior to exposure to the indicated drug concentrations, or vehicle. Wells were treated continuously for at least 2 weeks replacing media/drug every 3–4 days. Plates were fixed with tricyclic acid (10%), stained with sulforhodamine B (SRB) and absorbance measured. Absorbance for drug-treated wells was expressed relative to the control wells, with subtraction of the background SRB absorbance from an empty well. The mean of at least three replicate wells was calculated for each dose/combination.

Synergy was assessed using SRB absorbance from long-term clonogenic assays. Wells were treated every 3–4 days with palbociclib: 0, 100, 250, 500 or 750 nmol, and/or pictilisib: 0, 100, 200, 400, 500, or 1,000 nmol. For AZD2014, wells were treated every 3–4 days with palbociclib: 0, 100, 250, 500, or 750 nmol, and/or AZD2014: 0, 50, 100, 200, 400, and 750 nmol. Assessment of compound synergy was conducted using Bliss independence score. A Bliss additivity score of $\leq$1.0 was considered synergistic for that combination of drug concentrations. A cell line was considered to show drug synergy if at least three different combinations of drug concentrations were synergistic.

S-phase fraction was assayed after 24 or 72 hours exposure to compounds, with the addition of 10 μmol/L bromodeoxyuridine (BrdUrd) for 2 hours prior to fixing. BrdUrd incorporation was assessed with Cell Proliferation chemiluminescent ELISA-BrdUrd assay (Roche 11 669 915 001) according to the manufacturer's instructions and adjusted for viable cells in parallel wells assessed with CellTiter-Glo.

Tumor xenografts

In vivo efficacy and pharmacodynamic studies were approved by Genentech's Institutional Animal Care and Use Committee (IACUC) and adhered to the ILAR Guide for the Care and Use of Laboratory Animals. Naïve female C.B-17 SCID mice (Charles River Laboratories) were inoculated into the right 2/3 mammary fat pad with 2×10^7 MDA-MB-453 cells suspended in a 1:1 ratio of Hank's balanced salt solution and phenol red–free Matrigel (BD Biosciences). Once tumors reached a mean volume of about 300 mm^3, mice with similarly sized tumors were distributed into treatment cohorts ($n = 10$/group). Mice were dosed daily and orally, with vehicle [0.5% methylcellulose/0.2% tween-80 (MCT)], 5 mg/kg taselisib (GDC-0032), 50 mg/kg palbociclib, or the combination of taselisib and palbociclib for 21 consecutive days. Length (l) and width (w) of each tumor were measured using digital calipers (Fred V. Fowler Company, Inc.) and tumor volumes were calculated on the basis of the following formula: tumor volume $= l \times w^2 \times 0.5$.

Analysis of publicly available data sets

The METABRIC data set ($n = 1991$) was obtained by application to the European Genome-phenome archive (16). A total of 320 putative TNBC samples were normalized using the Beadarray package (17) and classified using TNBC type (18). Five samples were then removed as putative ER^+ samples leaving 315 for analysis. Segmented (CBS) copy number logR ratios were downloaded and used for copy number analysis, with gain/loss thresholds as defined previously (16). Heatmaps representing key cell-cycle genes were generated in R.

For 102 TCGA samples representing TNBC, level 3 RNA-seq data (raw gene counts) was downloaded from the TCGA web site for these samples. The gene counts were normalized using edgeR packages. Copy number, mutation, and RPPA data were extracted from cBioPortal using the CGDS-R (http://www.cbioportal.org/cgds_r.jsp). Additional data were downloaded from the Cancer Proteome Atlas project (17).

Statistical analysis

For *in vitro* studies, all statistical tests were performed with GraphPad Prism version 6.0. P values were two-tailed and considered significant if $P < 0.05$. Error bars represent SD or SEM of three experiments. Assessment of compound synergy was conducted using Bliss independence score.

Results

Luminal androgen receptor (LAR) subtype of TNBC is sensitive to CDK4/6 inhibition

We investigated whether the different molecular subgroups of TNBC were sensitive to CDK4/6 inhibition. Clonogenic assays were performed on a panel of 12 *RB1* wild-type TNBC cell lines and one *RB1*-mutant cell line (BT549), with the CDK4/6 inhibitor palbociclib (Fig. 1A and B). Cell lines from the dominant basal-like and mesenchymal (MES) subgroups of TNBC were resistant to palbociclib, whereas the LAR TNBC cell lines were highly sensitive to palbociclib ($P < 0.0001$ basal-like vs. LAR), and ribociclib (Fig. 1C), with sensitivity similar to the estrogen-positive cell line MCF7 (Fig. 1B). In BrdUrd proliferation assays, palbociclib had a substantially greater effect on S-phase entry in LAR cell lines compared with basal-like cell lines (Fig. 1D). The sensitivity of LAR tumors to palbociclib was investigated *in vivo* in MDA-MB-453 xenografts. Tumor reductions were observed after the initial nine days of consecutive dosing (palbociclib oral 50 mg/kg), with reduction in tumor size observed in 7 of 10 mice in the palbociclib treatment arm (Fig. 1E).

Palbociclib-sensitive cell lines have low postmitotic CDK2 activity

We hypothesized that sensitivity to CDK4/6 inhibition would be determined by the level of CDK2 activity after mitosis (12, 13). To investigate this, we used a live cell fluorescent sensor to measure CDK2 activity (CDK2L) in five *RB1* wild-type TNBC models (Fig. 2A). The CDK2L sensor specifically reports CDK2 activity, and is not phosphorylated by CDK4/6 and nor CDK1 (Materials and Methods).

We measured CDK2 activity in individual cells as they transitioned through mitosis and into the next cell cycle. Individual cells in the LAR palbociclib-sensitive cell lines MFM223 and MDA-MB-435, exited mitosis with low levels of CDK2 activity, which continued to fall during the first 2 hours after mitosis (Fig. 2B;

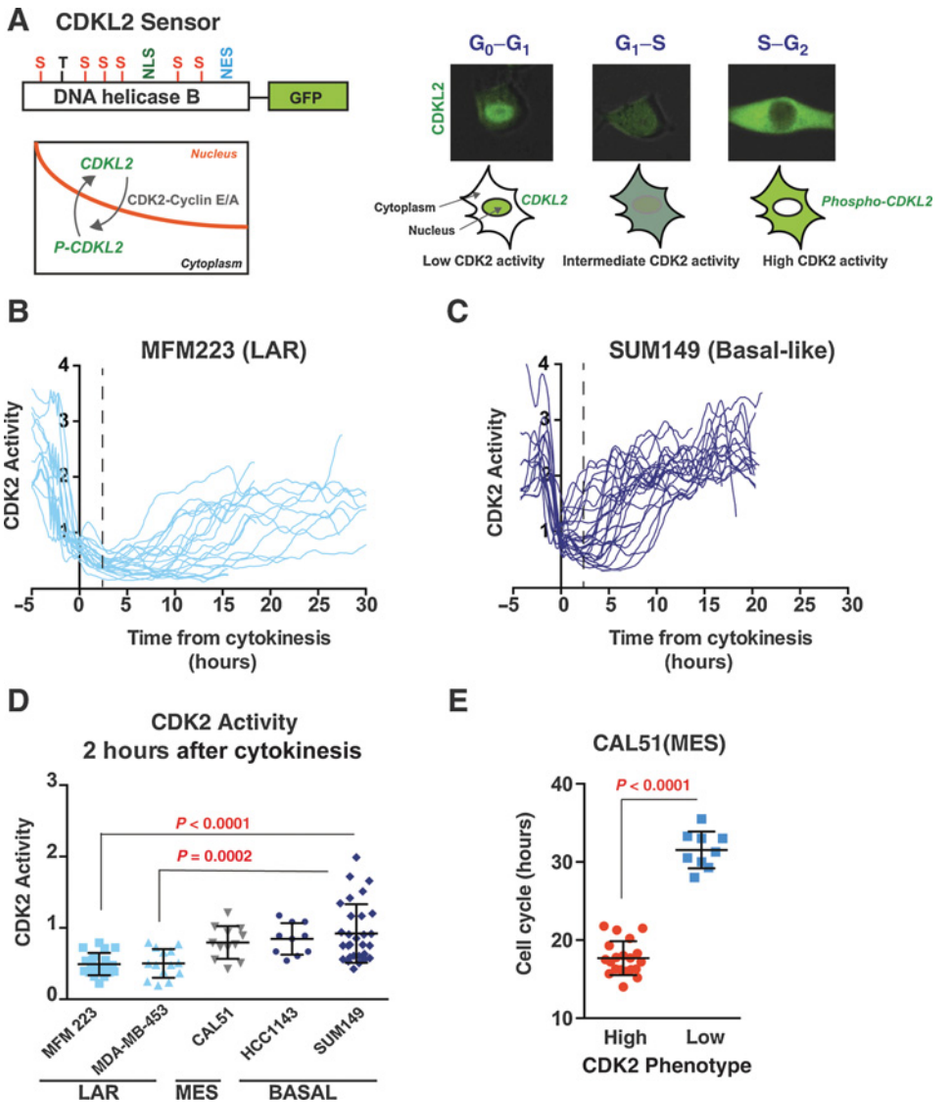

Figure 2.

Palbociclib-sensitive cell lines have low postmitotic CDK2 activity. **A,** An illustrative schematic of CDK2 activity live-cell sensor (CDK2L-GFP; left). CDK2 consensus phosphorylation sites shown: S, serine; T, threonine; NLS, nuclear localization signal; NES, nuclear export signal. Left, phosphorylation of CDK2L-GFP sensor by active CDK2 leads to export from the nucleus to the cytoplasm. Right, schematic diagram showing the changes in the sensor localization during the cell cycle. CDK2 activity is highest during S/G_2 phase of the cell cycle. Fluorescence images correspond to the CDKL2-GFP sensor in a single MFM223 cell. **B** and **C,** Single-cell CDK2 activity traces of palbociclib-sensitive LAR MFM223, $n = 20$ cells, 20% CDK2^{high} (**B**) and palbociclib-resistant basal-like SUM149, $n = 30$ cells, 74% CDK2^{high} (**C**). **D,** Postmitotic (2 hours after cytokinesis) CDK2 activity in individual cells from five TNBC cell lines. LAR MFM223 versus basal-like SUM149 cell lines (Student t test $P < 0.0001$). LAR MDA-MB-453 versus basal-like SUM149 ($P < 0.0002$). LAR, luminal androgen receptor subgroup (light blue); MES, mesenchymal (gray); and BASAL, basal-like (dark blue). **E,** Cell-cycle lengths (hours) in postmitotic CDK2^{high} versus CDK2^{low} subpopulations in CAL51 ($P < 0.0001$, Student t test).

Supplementary Fig. S1A). The dynamics of CDK2 activity after mitosis in the LAR cells were similar to CDK2 activity levels seen in the ER$^+$ MCF7 cell line (Supplementary Fig. S1B). In contrast, the palbociclib-resistant basal-like cell lines SUM149 and HCC1143 (Fig. 2C; Supplementary Fig. S1C), and the MES cell line CAL51 (Supplementary Fig. S1D), were predominately composed of cells that exited mitosis and started the next cell cycle with high baseline levels of CDK2 activity, which then rapidly accumulated.

To compare CDK2 activity between cell lines, CDK2 activity levels were quantified 2 hours after cytokinesis, the earliest timepoint that allowed accurate quantification after nuclear envelope reformation. Basal-like TNBC cell lines had significantly higher CDK2 activity compared with the LAR cell lines ($P < 0.0001$; Fig. 2D). Cells which exited mitosis with CDK2 activity <0.6 at 2 hours after cytokinesis were defined as CDK2^{low}, and cells with CDK2 activity >0.6 at 2 hours after cytokinesis were defined as CDK2^{high} (12). Whereas LAR cells exited mitosis with a relatively homogeneous CDK2^{low} phenotype, basal-like cells existed mitosis with heterogeneous levels of CDK2 activity including a large proportion of CDK2^{high} cells (Fig. 2D). In basal-like and MES cell lines, CDK2^{high} cells had substantially shorter cell cycles compared with CDK2^{low} cells ($P < 0.0001$; Fig. 2E; Supplementary Table S1). These results suggest that TNBC cell lines resistant to CDK4/6 inhibition are predominantly composed of actively proliferating CDK2^{high} cells, whereas TNBC cell lines sensitive to CDK4/6 inhibition were predominantly composed of more quiescent CDK2^{low} cells.

The proliferative CDK2^{high} subpopulation drives resistance to CDK4/6 inhibition at the single-cell level

We hypothesized that the CDK2^{high} subpopulation would be resistant to CDK4/6 inhibitors. The TNBC basal-like SUM149 model had a heterogeneous mix of CDK2 mitotic exit phenotypes with predominately CDK2^{high} cells and a smaller fraction of CDK2^{low} cells, and thus represented a good model to test this hypothesis. To assess the effect of palbociclib on the CDK2^{high} and CDK2^{low} populations, SUM149 cells expressing the CDK2L sensor were imaged for 8 hours prior to the addition of palbociclib or

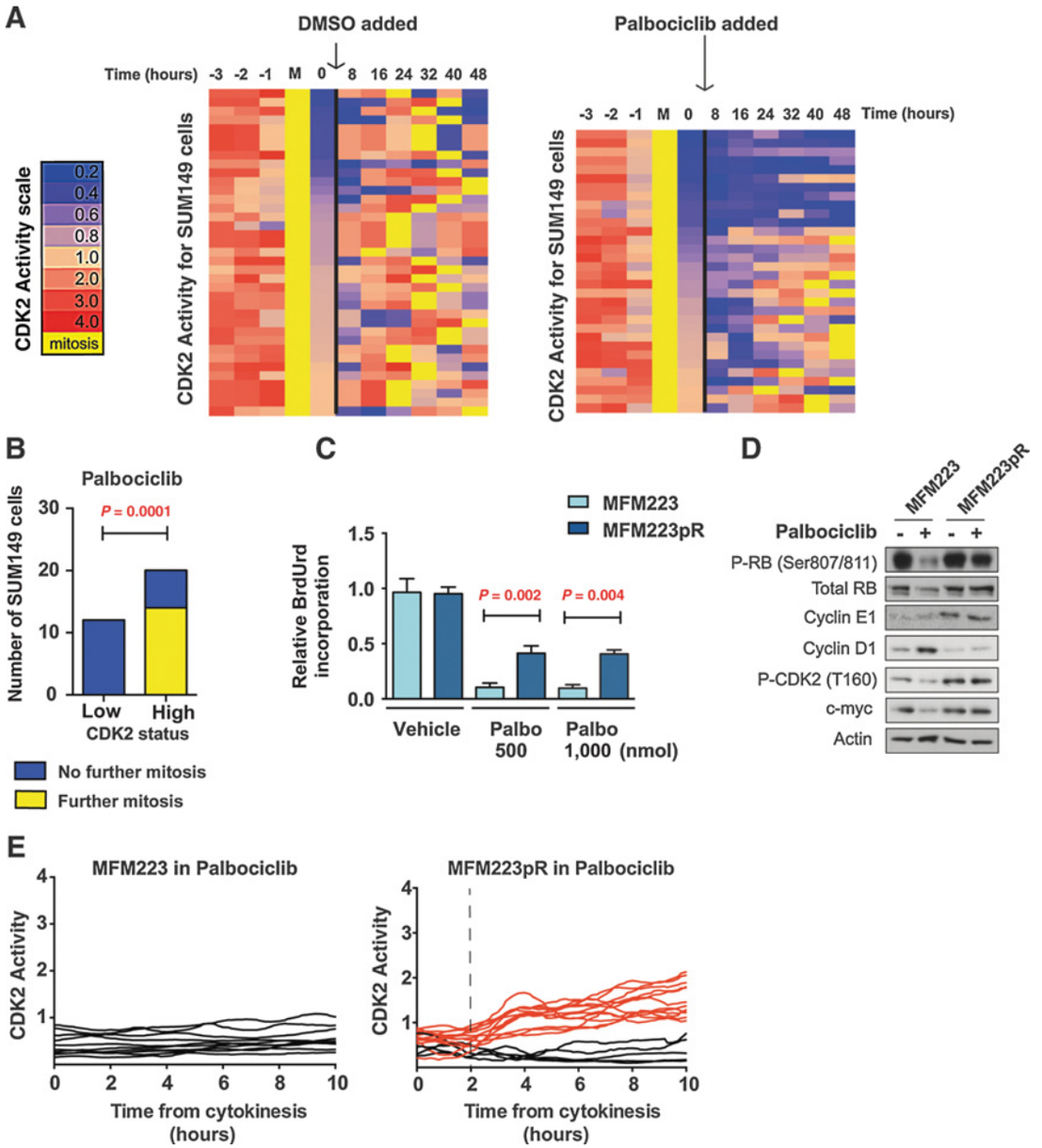

Figure 3.

The proliferative CDK2^{high} subpopulation drives resistance to CDK4/6 inhibition at the single-cell level. **A,** Cells with low CDK2 activity after mitosis do not reenter the cell cycle when exposed to palbociclib. Heatmap of CDK2 activity in individual SUM149 cells treated with vehicle (left; $n = 37$) or palbociclib (right; $n = 32$) added 1–3 hours after cytokinesis. CDK2 activity was synchronized and aligned *in silico* to point of cytokinesis (mitosis, M, yellow). T = 0 hours corresponds to CDK2 activity after cytokinesis and before palbociclib/vehicle addition. Each row represents one single cell. The heatmap is ordered according to levels of CDK2 activity after mitosis. **B,** Quantification of cells undergoing a second mitosis in SUM149 cells exposed to palbociclib 1–3 hours after mitosis as in CDK2^{high} versus CDK2^{low} (**A**). Cells that completed a second mitosis (yellow) versus those that did not underwent a second mitosis (blue) during the tracking period ($P = 0.0001$, Fisher exact test). **C,** Relative BrdUrd incorporation in MFM223 and MFM223pR treated with vehicle and palbociclib 500 nmol and 1,000 nmol for 72 hours (Student *t* test $P < 0.002$ and $P < 0.004$). **D,** Western blot of MFM223 and MFM223pR cells treated with vehicle or palbociclib 500 nmol for 72 hours and probed with the indicated antibodies. **E,** Single-cell CDK2 activity traces of cells grown in palbociclib 500 nmol; parental MFM223 (left); palbocicilb-resistant MFM223pR (right). Red, cells with CDK2 activity >1.0 at 10 hours (proliferating); black: cells with CDK2 activity <1.0 at 10 hours (quiescent).

vehicle, and only cells that completed cytokinesis 1–3 hours prior to palbociclib addition were tracked. CDK2 activity was assessed in individual cells for a further 48 hours after treatment (Materials and Methods). We observed that SUM149 cells that exited mitosis with a CDK2^{low} phenotype were blocked from entering the cell cycle by palbociclib over the 48 hours duration of time-lapse imaging (Fig. 3A). In contrast, cells that exited mitosis in a CDK2^{high} state successfully entered the cell cycle despite

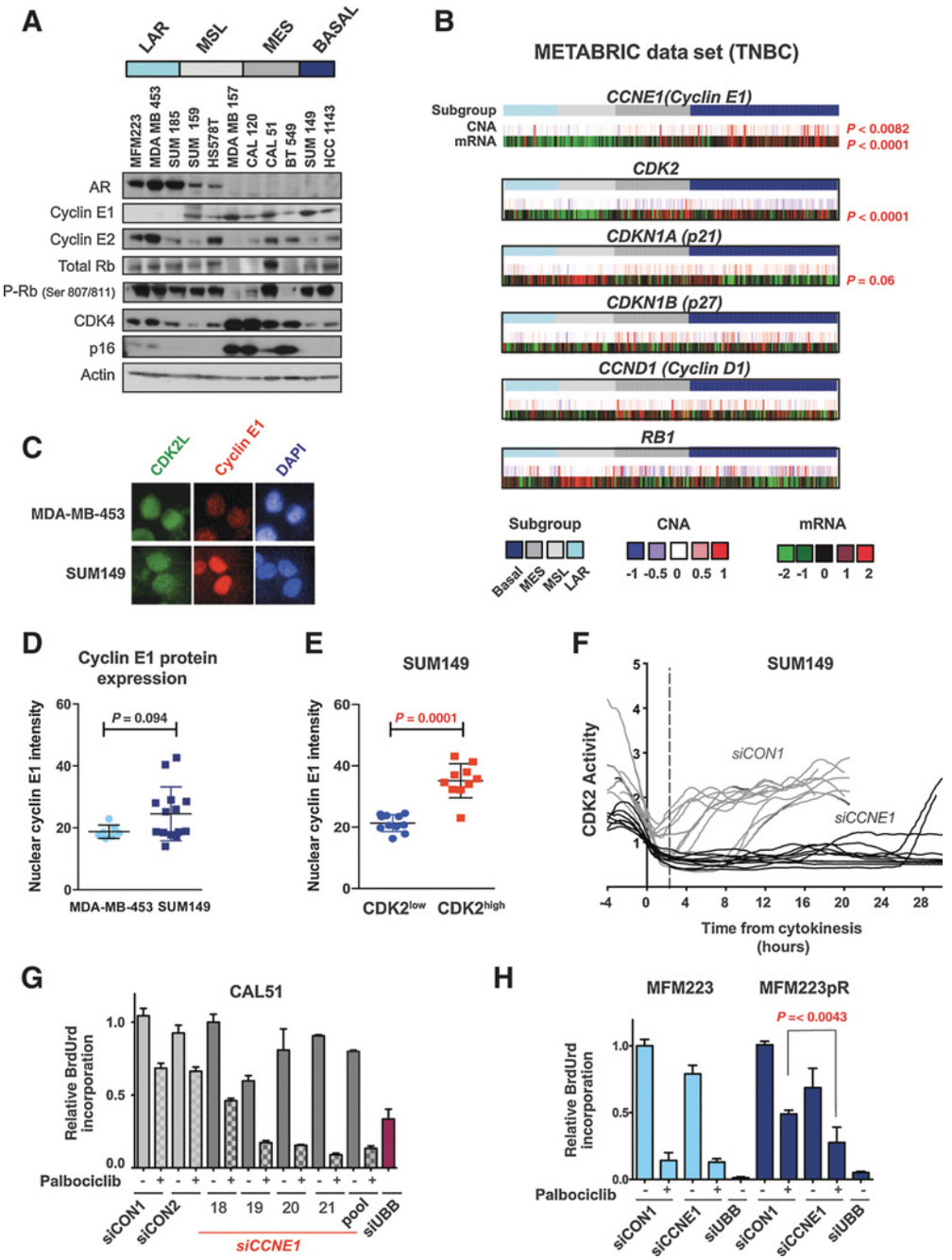

Figure 4.

High cyclin E1 expression after mitosis drives high CDK2 activity and CDK4/6 inhibitor resistance. **A,** Western blot of lysates from a panel of TNBC cell lines ($n = 11$ cell lines), probed with the indicated antibodies [not shown: densitometry for LAR vs. non-LAR for androgen receptor (AR) $P = 0.01$; Cyclin E1 $P = 0.02$; Mann–Whitney test]. **B,** Copy number aberrations (CNA, upper track) and gene expression (mRNA, lower track) from 219 primary TNBCs, clustered according to gene expression subtypes: LAR ($n = 35$); MSL ($n = 38$); MES ($n = 49$); basal-like ($n = 97$). *P* values generated from multiple *t* tests (1% false discovery rate) for gene expression comparisons LAR versus basal-like TNBC subtypes: Cyclin E1 (*CCNE1*) $P < 0.0001$; *CDK2* $P < 0.0001$; *CDKN1A* (p21) $P = 0.06$; *CDKN1B* (p27) $P = 0.23$. Copy number gain LAR versus basal-like: *CCNE1* $P = 0.0082$. Red, statistical significance. **C,** Immunofluorescent staining of nuclear cyclin E1 (red) in CDK2L-positive (GFP) MDA-MB-453 cells and SUM149 cells 1 hour after mitosis. DAPI (blue). **D,** Cyclin E1 nuclear intensity assessed by immunofluorescence and quantified with Columbus software in individual cells 1–2 hours after mitosis, in LAR MDA-MB-433 and basal-like SUM149 cell lines ($P = 0.094$, Student *t* test). **E,** Cyclin E1 nuclear intensity assessed by immunofluorescence in SUM149 cells 1–2 hours after cytokinesis in $CDK2^{low}$ versus $CDK2^{high}$ cells ($P < 0.0001$, Student *t* test). **F,** Single-cell CDK2 activity traces of proliferating SUM149 cells transfected 72 hours earlier with *siCON1* or *siCCNE1*. **G,** Relative BrdUrd incorporation in CAL51 cells transfected 72 hours earlier with *siCON1*, multiple individual *CCNE1* siRNAs and *siCCNE1* pool, treated with vehicle or palbociclib 500 nmol. **H,** Relative BrdUrd incorporation in MFM223 and MFM223pR cells transfected with the indicated siRNAs and treated with vehicle or palbociclib.

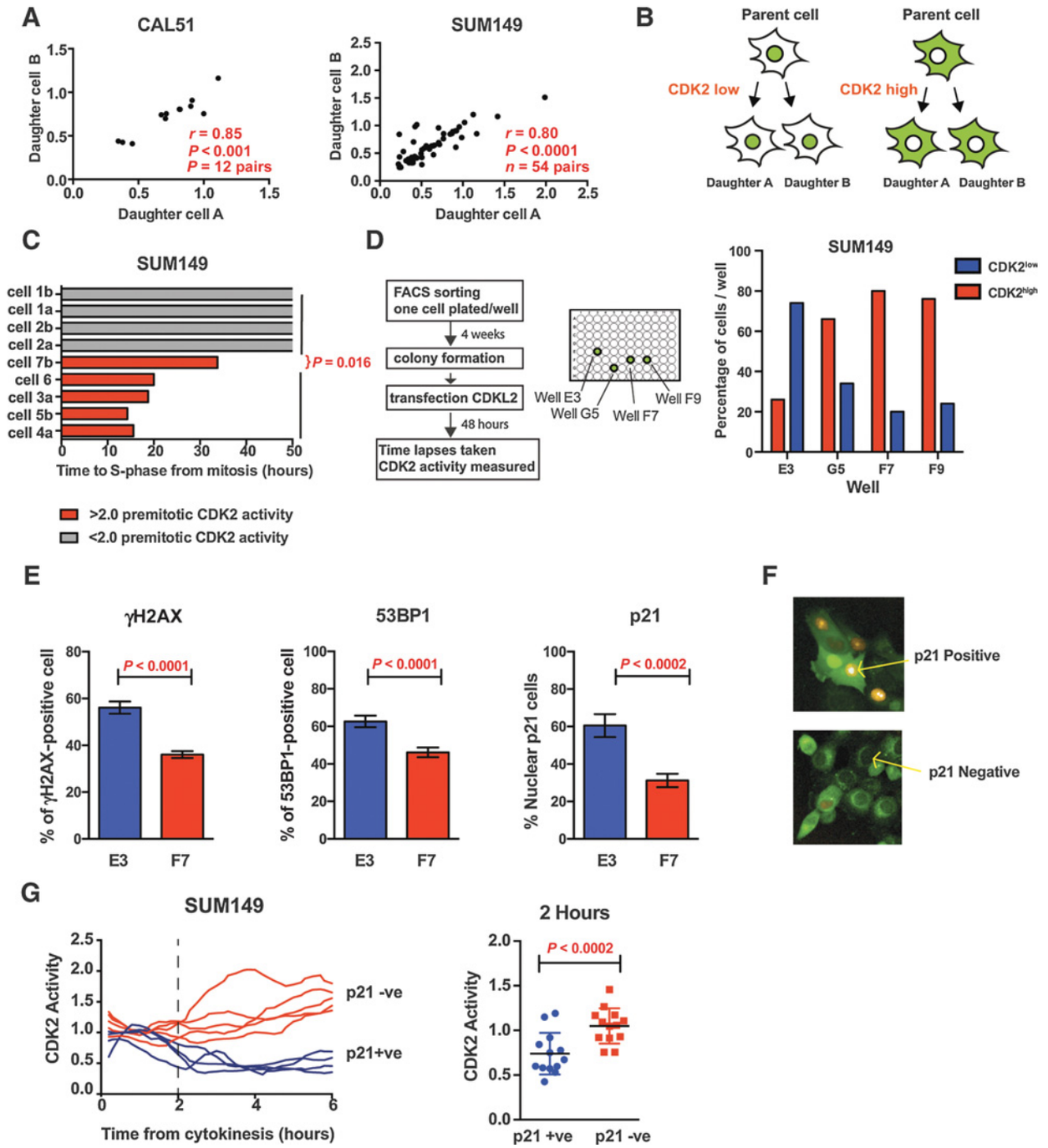

Figure 5.

Postmitotic CDK2 activity is determined before mitosis. **A,** Correlation of CDK2 activity 2 hours after cytokinesis between the daughter cell pairs generated in the same mitosis, in CAL51 (left) and SUM149 (right). **B,** Schematic illustrating shared levels of CDK2 activity between daughter cells. **C,** Time to S-phase entry for SUM149 cells that divided between 0 and 2 hours after palbociclib was added. Premitotic CDK activity (−2 hours) was measured in cells before palbociclib addition. Red, cells with premitotic CDK2 activity >2; gray, cells with premitotic activity <2.0, none of which entered S-phase by timepoint 50 hours after cytokinesis ($P = 0.016$, Mann–Whitney test). **D,** SUM149 cells were single-cell sorted by FACS and clones expanded from single cells for 4 weeks before transfection with CDK2L-GFP sensor (left). Percentage of $CDK2^{low}$ and $CDK2^{high}$ SUM149 cells per well, 50 cells tracked per well (right). **E,** Percentage of cell positive for γH2AX (E3 = total 860 cells; F7 = total 1508 cells), 53BP1 (E3 = total 719 cells; F7 = total 1,298 cells), and p21 (E3 = total 275 cells; F7 = total 539 cells) by immunofluorescence in the predominantly $CDK2^{low}$ E3 clones and $CDK2^{high}$ F7 clone. **F,** Immunofluorescence staining of p21 (yellow) in SUM149 cells transfected with CDK2 biosensor (green). **G,** CDK2 activity in SUM149 cell in relation to the p21 staining status at 6 hours after mitosis in SUM149 cells. Left, CDK2 activity traces; right, CDK2 activity at 2 hours after cytokinesis in p21-positive and p21-negative cells.

palbociclib treatment and subsequently underwent a second mitosis (Fig. 3A and B). Therefore, although the SUM149 cell line was intrinsically resistance to palbociclib in long-term clonogenic assays, the subfraction of CDK2^{low} cells were sensitive to palbociclib. Palbociclib did prolong cell-cycle length in CDK2^{high} cells (mean cell-cycle length 20 hours vehicle vs. 38 hours palbociclib, Fig. 3A) suggesting that CDK4/6 did facilitate, but was not essential for S-phase entry. After 14 days of chronic treatment with palbociclib, the cell-cycle length for the SUM149 cells returned toward pretreatment levels, suggesting adaption to CDK4/6 inhibition (Supplementary Fig. S1E and S1F). Collectively, these data demonstrate that postmitotic CDK2 activity dictates sensitivity to CDK4/6 inhibition. CDK2^{high} cells have sufficient CDK2 activity to bypass the restriction point, the point where CDK4/6 activity is necessary for cell-cycle reentry, resulting in CDK4/6 inhibitor resistance.

We next established whether CDK2 activity at mitotic exit changed after developing acquired resistance to CDK4/6 inhibitors in the LAR cell lines. We generated palbociclib-resistant cells from the MFM223 cell line (MFM223pR) via four months of chronic palbociclib exposure. In clonogenic assays, the MFM223pR cells were resistant to palbociclib, with a greater proportion of cells in S-phase during palbociclib treatment compared with the parental palbociclib-sensitive cell line MFM223 (Fig. 3C). The MFM223pR model acquired higher protein levels of cyclin E1 and activating CDK2 T160 phosphorylation (Fig. 3D). In MFM223pR cells, a new CDK2^{high} proliferative subpopulation emerged (Fig. 3E), suggesting that the mechanism of acquired resistance to palbociclib was due to a higher proportion of cells adopting the CDK2^{high} phenotype.

Temporal dysregulation of cyclin E1 expression in TNBC cells drives higher CDK2 activity after mitosis

To explore the molecular determinants of CDK2^{high} cells, we profiled our panel of TNBC cell lines. The LAR cell lines had both high expression of the androgen receptor (AR; $P = 0.01$) and absent/low expression of cyclin E1 ($P = 0.02$; Fig. 4A). We profiled TNBC tumors using publicly available data sets. In both the METABRIC (16) and TCGA (19) data sets, TNBC LAR tumors had significantly lower transcriptomic expression levels of *CCNE1* ($P < 0.0001$) and *CDK2* ($P < 0.0001$), with higher *CDKN1A* (p21) levels, as compared with basal-like TNBC ($P = 0.06$; Fig. 4B; Supplementary Fig. S2A and S2B). Basal-like TNBC tumors frequently had increased *CCNE1* gene copy number than observed in the LAR tumors ($P = 0.008$ Fisher exact test, Fig. 4B). There was a high correlation between cyclin E1 mRNA with protein levels ($r = 0.89$; Supplementary Fig. S2C and S2D).

Cyclin E1 is tightly regulated nuclear protein, periodically expressed during the cell cycle, with the highest levels occurring during late G_1 and early S-phase in noncancer models (20). We investigated the temporal regulation of cyclin E1 in palbociclib-sensitive and resistant cell lines, to assess whether deregulation of cyclin E1 expression in early G_1 promoted the CDK2^{high} population. To test this, we assessed the expression of nuclear cyclin E1 protein in individual cells 1–2 hours after mitosis by dual immunofluorescence with the CDK2L sensor (see Materials and Methods). Basal-like SUM149 cells had aberrantly high cyclin E1 expression after mitosis (Fig. 4C and D; Supplementary Fig. S2E) compared with the LAR MDA-MB-453 cells that had uniformly low cyclin E1 expression. This was substantially earlier than the time point where SUM149 cells typically entered S-phase, confirmed by using a PCNA sensor (Supplementary Fig. S2F). CDK2^{high} SUM149 cells had higher levels of cyclin E1 protein expression than CDK2^{low} SUM149 cells (Fig. 4E). Silencing of cyclin E1 in SUM149 cells resulted in the loss of the CDK2^{high} population after mitosis and induced a CDK2^{low} phenotype (Fig. 4F; Supplementary Fig. S2G). Furthermore, silencing of cyclin E1 sensitized CAL51 (Fig. 4G; Supplementary Fig. S2H), SUM149 (Supplementary Fig. S2I), and MFM223pR cells to palbociclib, with minimal effects upon parental MFM223 cells, which had low levels of cyclin E1 expression (Fig. 4H). Silencing of cyclin E1 in the absence of CDK4/6 inhibition did not substantially reduce BrdUrd incorporation, likely due to redundancy between different CDKs and cyclins. Our data suggested that aberrant expression of cyclin E1 immediately after mitosis, promoted the CDK2^{high} phenotype and resistance to CDK4/6 inhibition.

The CDK2^{high} phenotype is determined before mitosis

We next addressed whether postmitotic activity was determined before mitosis, as previously shown in noncancer models (12). SUM149 and CAL51 sister cell pairs, generated from the same mitosis, shared similar postmitotic CDK2 activity (Fig. 5A and B) suggesting that the level of CDK2 activity after mitosis was determined prior to cytokinesis. SUM149 cells with higher premitotic CDK2 activity (2 hours prior to mitosis) generated daughter cells that entered S-phase despite CDK4/6 inhibition (Fig. 5C), whereas cells with lower premitotic CDK2 activity were arrested by CDK4/6 inhibition ($P = 0.016$).

Having demonstrated that postmitotic CDK2 activity was determined precytokinesis, we investigated whether this was due to the existence of a fixed subpopulation of CDK2^{high} cells, or whether CDK2^{high} and CDK2^{low} populations could interconvert. To test the long-term stability of the CDK2^{low} and CDK2^{high} subpopulations, we FACS-sorted single cells from the SUM149 cell line (Fig. 5D) and CAL51 cell line (Supplementary Fig. S3A) into 96-well plates, confirmed single-cell seeding by microscopy, and assessed CDK2 activity in the resulting single-cell clones after four weeks of multiplication. In general, clonal populations recapitulated variability in CDK2^{high} and CDK2^{low} populations despite arising from a single cell (Fig. 5D; Supplementary Fig. S3). The fraction of CDK2^{high} cells was the most prevalent phenotype (50 cells measured/well) across three of the four wells imaged in SUM149. In contrast, we identified a clonal SUM149 population that was robustly CDK2^{low} (well E3) at a single time point, 2 hours after cytokinesis, although it was not addressed whether greater heterogeneity in CDK2 activity could develop over time. Overall, these results suggest that postmitotic CDK2^{high} activity is determined before mitosis, but the CDK2^{high} and CDK2^{low} subpopulations are not distinct fixed populations, with cells interconverting between the 2 phenotypes over many generations.

The SUM149 cells have a *BRCA1* mutation (21), which may have elevated levels of DNA damage. We hypothesized that the E3 clone, which maintained a large population of CDK2^{low} cells, may have increased levels of DNA damage. Immunofluorescence staining for markers of DNA damage revealed that the SUM149 E3 clonal cell population, had a higher percentage of γH2AX-, 53BP1-, and p21-positive cells, compared with the F7 clonal population (Fig. 5E and F). Parental SUM149 cells that exited mitosis with CDK2^{low} phenotype were p21 positive by

immunofluorescence (Fig. 5G), as previously observed in noncancer models (12). These results suggest that DNA damage and p21 expression may in part determine CDK2 activity state at mitotic exit (22).

Inhibition of PI3 kinase signaling is synergistic with CDK4/6 inhibitors, in *PIK3CA*-mutant TNBC models

The nonbasal, LAR, and MSL subtypes of TNBC are substantially enriched with activating mutations in the PI3K catalytic subunit *PIK3CA* gene (7), and therefore we investigated the therapeutic potential of inhibiting the PI3K pathway in TNBC. A synergistic interaction (Bliss additivity score < -1.0) was observed between the pan class I PI3K inhibitor pictilisib (GDC0941) and palbociclib in *PIK3CA*-mutant TNBC cell lines (Fig. 6A), as recently reported by others and us in ER^+ cell lines (10, 23) and the MDA-MB-453 LAR cell line (23). Combination synergy was not observed in *PIK3CA* wild-type cell lines nor the *RB1*-mutant cell line BT549. Synergy was also observed with mTOR inhibitor AZD2014–palbociclib combinations in *PIK3CA* mutant and some *PIK3CA* wild-type TNBC cell lines (Supplementary Fig. S4A). We further validated the efficacy of the drug combination with the-selective PI3K inhibitor taselisib (GDC0032), which substantially sensitized the MSL cell line SUM159 to palbociclib in clonogenic assays (Fig. 6B) and BrdUrd proliferation assays (Supplementary Fig. S4B). This data suggested that combinations of PI3K pathway inhibitors and CDK4/6 inhibitors could extend the utility of CDK4/6 inhibitors outside LAR subtype cancers.

The combination of palbociclib and taselisib demonstrated greater efficacy than either compound alone in xenografts from the *PIK3CA*-mutant LAR MDA-MB-453 cell line (palbociclib vs. combination $P = 0.02$; taselisib vs. combination $P = 0.01$; Fig. 6C). Pharmacodynamic studies at 1-hour and 4-hour timepoints in the mouse tumors from MDA-MB-453 xenografts treated with individual drugs or the combination, demonstrated significant reduction in phosphorylated RB1 compared with vehicle (Fig. 6D; vehicle vs. taselisib 1 hour $P = 0.0004$, 4 hours $P < 0.0001$; vehicle vs. palbociclib 1 hour $P < 0.0001$, 4 hours $P < 0.0001$; vehicle vs. combination 1 hour $P < 0.0001$, 4 hours $P < 0.0001$). The combination induced greater levels of apoptosis than either drug alone (Supplementary Fig. S4C).

Finally, we examined whether PI3K inhibition with taselisib affected postmitotic CDK2 levels using the *PIK3CA*-mutant MES CAL51 cell line. Taselisib decreased postmitotic CDK2 activity with a greater proportion of cells exiting mitosis with the $CDK2^{low}$ phenotype (Fig. 6E). Premitotic CDK2 levels influenced entry into the cell-cycle after mitosis (Supplementary Fig. S4D). This data suggested that inhibition of PI3K signaling sensitized to CDK4/6 inhibition, in part, as PI3K inhibition suppressed postmitotic CDK2 activity, inducing a $CDK2^{low}$ quiescent state where CDK4/6 activity was required to initiate the cell cycle.

Discussion

We have shown that the LAR subgroup of triple negative breast cancers (TNBC) is highly sensitive to CDK4/6 inhibition *in vitro* and *in vivo* (Fig. 1). Sensitivity to CDK4/6 inhibition is dictated at the single-cell level, with resistance to CDK4/6 inhibitors arising from cancer cells that exit mitosis directly into a $CDK2^{high}$ proliferative state, from which CDK4/6 is not necessary for cell-cycle reentry (Figs. 2C and 3A).

Our results further extend prior work in noncancer models that demonstrate a biphasic exit of cells into proliferative and quiescent states after mitosis (12, 13). Cells that exit mitosis with a $CDK2^{low}$ phenotype enter into a quiescent state, requiring CDK4/6 activity to initiate reentry into the cell cycle (Fig. 6F), and are hence sensitivity to CDK4/6 inhibition. In contrast, cells that exit mitosis with a $CDK2^{high}$ phenotype enter into a proliferative state, bypassing the restriction point (Fig. 6G), with shorter doubling times. Tumors with a high proportion of $CDK2^{high}$ cells are resistant to CDK4/6 inhibition. Palbociclib-sensitive LAR cancer cells typically exit into a quiescent $CDK2^{low}$ state after mitosis, from which CDK4/6 is required to phosphorylate RB1 and pass the restriction point (2, 24–27). In contrast, basal-like TNBC cells frequently enter a proliferative $CDK2^{high}$ state and are thus resistant to palbociclib treatment. This provides a mechanistic explanation for why basal-like, and potentially many other tumor types are resistant to CDK4/6 inhibition despite being RB1 wild-type. The CDK4/6 and PI3 kinase inhibitor combinations have substantial activity in *PIK3CA*-mutant nonbasal TNBC, of both LAR and mesenchymal-stem (MSL) subgroups (Fig. 6A), with such combinations having the potential to further expand the TNBC subgroups that could benefit from CDK4/6 inhibition.

Cyclin E1 binds to and activates CDK2 (28, 29) and prior work has demonstrated that cyclin E1 expression mediates resistance to CDK4/6 inhibition (10, 30). The classical view is that CDK2 and cyclin E are downstream of CDK4/6 activity (24). Here we show that in palbociclib-resistant TNBC, cyclin E1 expression is dysregulated and expressed immediately after mitosis (Fig. 4D). Dysregulation of cyclin E1 promotes the $CDK2^{high}$ phenotype, with the CDK2–CyclinE complex active immediately after mitosis, resulting in a short G_1 phase (Fig. 6G). The SUM149 cells harbor an inactivating *FBXW7* mutation that disrupts the SCF complex, probably contributing to the dysregulation of cyclin E1 expression (Supplementary Table S2). In other contexts, increased *CCNE1* gene copy number may drive dysregulation of cyclin E1 expression after mitosis (10). These observations suggest that the measurement of cyclin E1 expression either at the RNA or protein level has the potential to be utilized as a predictive biomarker of resistance to CDK4/6 inhibition in breast cancer.

Daughter cells share the same CDK2 activity state, suggesting that postmitotic CDK2 activity is determined before mitosis (Fig. 5A). However, this is not the result of $CDK2^{high}$ and $CDK2^{low}$ cells, as colonies derived from individual cells largely recapitulate the same variability in CDK2 activity as the parental cell line (Fig. 5D). We provide some data to suggest that DNA damage, and the resulting induction of p21 expression, may also regulate CDK2 activity state after mitosis (Fig. 5G). However, more research is required to further assess the potential role of DNA damaging signaling in this context.

Our results illustrate how single-cell analysis can identify mechanisms of resistance to targeted therapies. Phenotypic heterogeneity between single cells may drive drug resistance, and this may be more clearly elucidated at the single-cell level than through assessment of bulk cell populations. Through single-cell approaches, we identify that CDK2 activity after mitosis is a key determinant of sensitivity to CDK4/6 inhibition, and highlight potential therapeutic strategies for TNBC. An ongoing therapeutic trial is assessing the effectiveness of CDK4/6 inhibition in

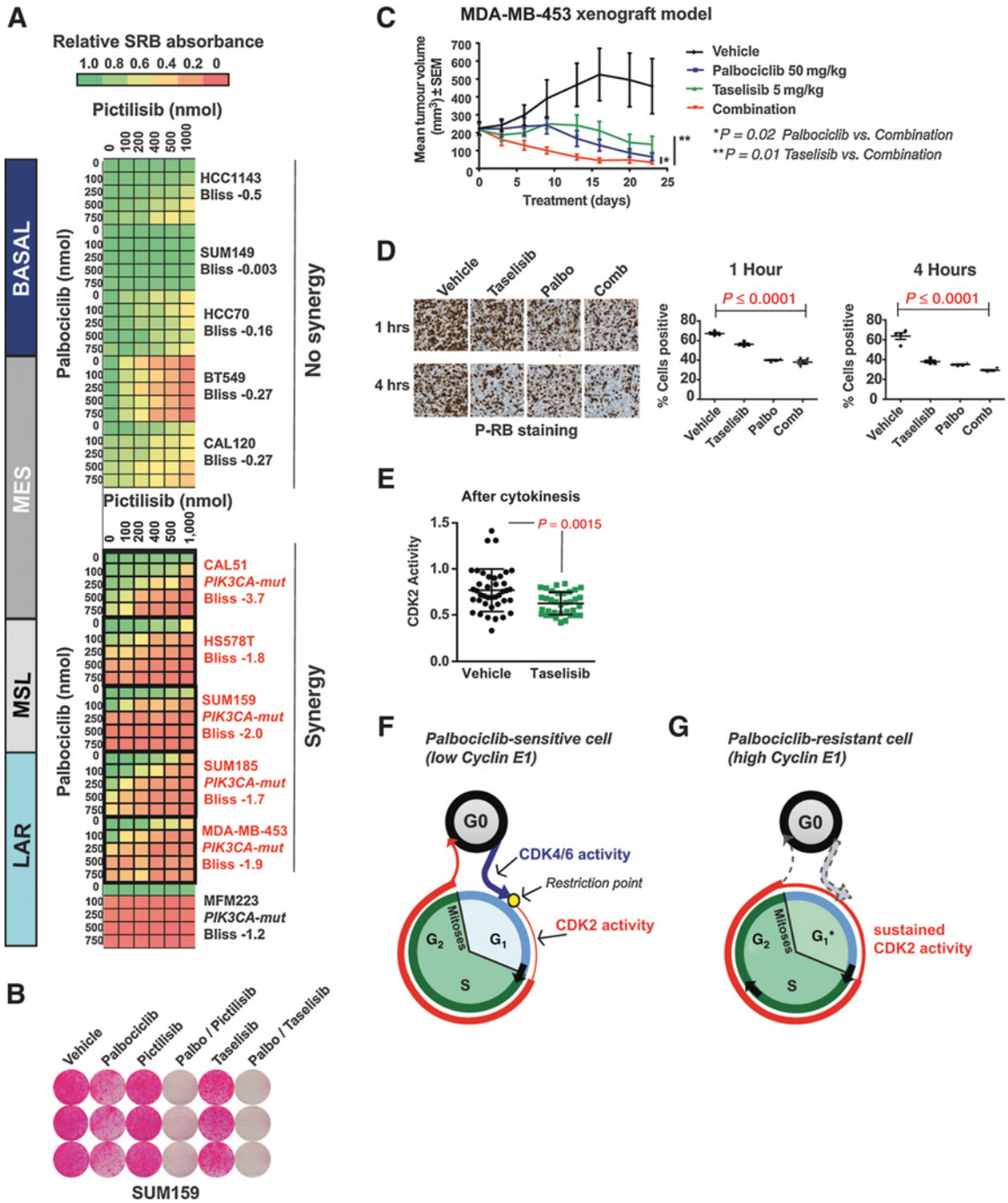

Figure 6.

Inhibition of PI3K signaling synergizes with CDK4/6 inhibition in *PIK3CA*-mutant TNBC. **A,** Synergy heatmap matrices of clonogenic assays in TNBC cell lines treated with palbociclib and/or pictilisib (PI3K inhibitor) at increasing concentrations. Red, cell lines with combination synergy assessed using Bliss additivity score. *PIK3CA* mut, *PIK3CA* mutant. The lowest Bliss additivity score for each cell line is indicated. **B,** Clonogenic assays in *PIK3CA*-mutant SUM159 MSL TNBC cell line grown in palbociclib 500 nmol, pictilisib (pan-PI3 kinase inhibitor) 200 nmol, taselisib (alpha-specific PI3K inhibitor) 100 nmol, and indicated combinations. **C,** Mouse xenografts of LAR MDA-MB-453 cells, treated daily with vehicle ($n = 10$), palbociclib ($n = 10$), taselisib ($n = 10$), or combination ($n = 10$; $P = 0.02$ palbociclib vs. combination $P = 0.02$; taselisib vs. combination $P = 0.01$). Error bars are mean tumor volume and SD. **D,** Left, IHC of MDA-MB-453 mouse xenografts stained for phosphorylated RB1 (Ser807/811) after 1 and 4 hours of indicated drug treatment(s). Right, Scatter plots with percentage of positively stained cells for phosphorylated RB1 in IHC sections (left) after 1 hour and 4 hours of treatment. **E,** CDK2 activity after mitosis in *PIK3CA*-mutant CAL51 treated with vehicle or taselisib 100 nmol. **F,** Model of cell-cycle dynamics in $CDK2^{low}$ cells. Cell exit mitosis into a quiescent state with CDK4/6 activity (blue) necessary to pass through the restriction point (yellow circle), after which CDK2 activity (red) promotes S-phase entry. **G,** Model of cell-cycle dynamics in $CDK2^{high}$ cells. Cells exit mitosis into an active proliferating state with high CDK2 activity, bypassing the restriction point, and CDK4/6 activity is not necessary to enter S-phase. Consequently, $CDK2^{high}$ cells, and cancers with a high proportion of $CDK2^{high}$ cells, are resistant to CDK4/6 inhibition.

combination with PI3K inhibition, in patients with *PIK3CA*-mutant TNBC (NCT02389842).

Disclosure of Potential Conflicts of Interest

N.C. Turner is a consultant/advisory board member for and reports receiving commercial research grants from Genentech and Pfizer. No potential conflicts of interest were disclosed by the other authors.

Authors' Contributions

Conception and design: U.S. Asghar, D. Sampath, M.T. Herrera-Abreu, N.C. Turner

Development of methodology: U.S. Asghar, A.R. Barr, J. Giltnane, A. Pearson, M.T. Herrera-Abreu

Acquisition of data (provided animals, acquired and managed patients, provided facilities, etc.): U.S. Asghar, A.R. Barr, M. Beaney, I. Babina, D. Sampath, J. Giltnane, J.A. Lacap, L. Crocker, A. Young, A. Pearson, M.T. Herrera-Abreu

Analysis and interpretation of data (e.g., statistical analysis, biostatistics, computational analysis): U.S. Asghar, A.R. Barr, R. Cutts, D. Sampath, J. Giltnane, M.T. Herrera-Abreu, N.C. Turner

Writing, review, and/or revision of the manuscript: U.S. Asghar, A.R. Barr, D. Sampath, M.T. Herrera-Abreu, C. Bakal, N.C. Turner

Administrative, technical, or material support (i.e., reporting or organizing data, constructing databases): U.S. Asghar, I. Babina, J.A. Lacap, L. Crocker, M.T. Herrera-Abreu

Study supervision: D. Sampath, M.T. Herrera-Abreu, N.C. Turner

Acknowledgments

The authors acknowledge Frederick Wallberg and Rhadhika Patel for flow cytometry support services and Vicky Bousgouni for live imaging support. The authors also acknowledge NHS funding to the NIHR Biomedical Research Centre at The Royal Marsden and the ICR.

Grant Support

This research was funded by the Avon Foundation (to U.S. Asghar), Breast Cancer Now with generous support from the Mary-Jean Mitchell Green Foundation and Cancer Research UKC30746/A16642 (to N.C. Turner).

The costs of publication of this article were defrayed in part by the payment of page charges. This article must therefore be hereby marked *advertisement* in accordance with 18 U.S.C. Section 1734 solely to indicate this fact.

Received February 7, 2017; revised April 13, 2017; accepted June 5, 2017; published OnlineFirst June 12, 2017.

References

1. Hanahan D, Weinberg RA. Hallmarks of cancer: the next generation. Cell 2011;144:646–74.
2. Asghar U, Witkiewicz AK, Turner NC, Knudsen ES. The history and future of targeting cyclin-dependent kinases in cancer therapy. Nat Rev Drug Discov 2015;14:130–46.
3. Finn RS, Crown JP, Lang I, Boer K, Bondarenko IM, Kulyk SO, et al. The cyclin-dependent kinase 4/6 inhibitor palbociclib in combination with letrozole versus letrozole alone as first-line treatment of oestrogen receptor-positive, HER2-negative, advanced breast cancer (PALOMA-1/TRIO-18): a randomised phase 2 study. Lancet Oncol 2015;16:25–35.
4. Turner NC, Ro J, Andre F, Loi S, Verma S, Iwata H, et al. Palbociclib in hormone-receptor-positive advanced breast cancer. N Engl J Med 2015;373:209–19.
5. Finn RS, Martin M, Rugo HS, Jones S, Im SA, Gelmon K, et al. Palbociclib and letrozole in advanced breast cancer. N Engl J Med 2016;375:1925–36.
6. Hortobagyi GN, Stemmer SM, Burris HA, Yap YS, Sonke GS, Paluch-Shimon S, et al. Ribociclib as first-line therapy for HR-positive, advanced breast cancer. N Engl J Med 2016;375:1738–48.
7. Lehmann BD, Bauer JA, Chen X, Sanders ME, Chakravarthy AB, Shyr Y, et al. Identification of human triple-negative breast cancer subtypes and preclinical models for selection of targeted therapies. J Clin Invest 2011;121:2750–67.
8. Burstein MD, Tsimelzon A, Poage GM, Covington KR, Contreras A, Fuqua SA, et al. Comprehensive genomic analysis identifies novel subtypes and targets of triple-negative breast cancer. Clin Cancer Res 2015;21:1688–98.
9. Finn RS, Dering J, Conklin D, Kalous O, Cohen DJ, Desai AJ, et al. PD 0332991, a selective cyclin D kinase 4/6 inhibitor, preferentially inhibits proliferation of luminal estrogen receptor-positive human breast cancer cell lines in vitro. Breast Cancer Res 2009;11:R77.
10. Herrera-Abreu MT, Palafox M, Asghar U, Rivas MA, Cutts RJ, Garcia-Murillas I, et al. Early adaptation and acquired resistance to CDK4/6 inhibition in estrogen receptor-positive breast cancer. Cancer Res 2016;76:2301–13.
11. Barr AR, Heldt FS, Zhang T, Bakal C, Novak B. A dynamical framework for the all-or-none G1/S transition. Cell Syst 2016;2:27–37.
12. Spencer SL, Cappell SD, Tsai FC, Wesley Overton K, Wang CL, Meyer T. The proliferation-quiescence decision is controlled by a bifurcation in CDK2 activity at mitotic exit. Cell 2013;155:369–83.
13. Cappell SD, Chung M, Jaimovich A, Spencer SL, Meyer T. Irreversible APC (Cdh1) inactivation underlies the point of no return for cell-cycle entry. Cell 2016;166:167–80.
14. Pearson A, Smyth E, Babina IS, Herrera-Abreu MT, Tarazona N, Peckitt C, et al. High-level clonal FGFR amplification and response to FGFR inhibition in a translational clinical trial. Cancer Discov 2016;6:838–51.
15. Piatkevich KD, Hulit J, Subach OM, Wu B, Abdulla A, Segall JE, et al. Monomeric red fluorescent proteins with a large Stokes shift. Proc Natl Acad Sci U S A 2010;107:5369–74.
16. Curtis C, Shah SP, Chin SF, Turashvili G, Rueda OM, Dunning MJ, et al. The genomic and transcriptomic architecture of 2,000 breast tumours reveals novel subgroups. Nature 2012;486:346–52.
17. Dunning MJ, Smith ML, Ritchie ME, Tavare S. beadarray: R classes and methods for Illumina bead-based data. Bioinformatics 2007;23:2183–4.
18. Chen X, Li J, Gray WH, Lehmann BD, Bauer JA, Shyr Y, et al. TNBCtype: a subtyping tool for triple-negative breast cancer. Cancer Inform 2012;11:147–56.
19. The Cancer Genome Atlas Network. Comprehensive molecular portraits of human breast tumours. Nature 2012;490:61–70.
20. Le Cam L, Polanowska J, Fabbrizio E, Olivier M, Philips A, Ng Eaton E, et al. Timing of cyclin E gene expression depends on the regulated association of a bipartite repressor element with a novel E2F complex. EMBO J 1999;18:1878–90.
21. Elstrodt F, Hollestelle A, Nagel JH, Gorin M, Wasielewski M, van den Ouweland A, et al. BRCA1 mutation analysis of 41 human breast cancer cell lines reveals three new deleterious mutants. Cancer Res 2006;66:41–5.
22. Barr AR, Cooper S, Heldt FS, Butera F, Stoy H, Mansfeld J, et al. DNA damage during S-phase mediates the proliferation-quiescence decision in the subsequent G1 via p21 expression. Nat Commun 2017;8:14728.
23. Vora SR, Juric D, Kim N, Mino-Kenudson M, Huynh T, Costa C, et al. CDK 4/6 inhibitors sensitize PIK3CA mutant breast cancer to PI3K inhibitors. Cancer Cell 2014;26:136–49.
24. Harbour JW, Luo RX, Dei Santi A, Postigo AA, Dean DC. Cdk phosphorylation triggers sequential intramolecular interactions that progressively block Rb functions as cells move through G1. Cell 1999;98:859–69.
25. Ezhevsky SA, Nagahara H, Vocero-Akbani AM, Gius DR, Wei MC, Dowdy SF. Hypo-phosphorylation of the retinoblastoma protein (pRb) by cyclin D:Cdk4/6 complexes results in active pRb. Proc Natl Acad Sci U S A 1997;94:10699–704.
26. Lundberg AS, Weinberg RA. Functional inactivation of the retinoblastoma protein requires sequential modification by at least two distinct cyclin-cdk complexes. Mol Cell Biol 1998;18:753–61.
27. O'Leary B, Finn RS, Turner NC. Treating cancer with selective CDK4/6 inhibitors. Nat Rev Clin Oncol 2016;13:417–30.
28. Dulic V, Lees E, Reed SI. Association of human cyclin E with a periodic G1-S phase protein kinase. Science 1992;257:1958–61.
29. Koff A, Giordano A, Desai D, Yamashita K, Harper JW, Elledge S, et al. Formation and activation of a cyclin E-cdk2 complex during the G1 phase of the human cell cycle. Science 1992;257:1689–94.
30. Taylor-Harding B, Aspuria PJ, Agadjanian H, Cheon DJ, Mizuno T, Greenberg D, et al. Cyclin E1 and RTK/RAS signaling drive CDK inhibitor resistance via activation of E2F and ETS. Oncotarget 2015;6:696–714.